Zhaowen YAN, Wenlu YU, Jin CAO, Yansheng WANG, Yajing HAN, Toyobur RAHMAN

Beihang University

A Novel EBG Structure with Embedded Meander Bridge and Its Applications on SI and PI

Abstract. *This paper proposes an embedded meander bridge planar EBG structure, which can effectively suppress ultra-wideband (UWB) simultaneous switching noise (SSN) in power/ground plane pairs. This paper demonstrates that the valid -30 dB suppression bandwidth of the novel EBG structure is from 500 MHz to 14.5 GHz, covering a range of 14GHz. Furthermore, the effects of the EBG power plane on signal integrity (SI) is investigated. The design rules of the signal lines over the EBG power/ground plane pairs are also studied. The simulated and measured results are compared to verify the performance.*

Streszczenie. *W artykule opisano mostkową strukture EBG typu meander która umożliwia skuteczne tłumienie szumów szerokopasmowych. Układ umożliwia tłumienie o 30 dB sygnałów w paśmie 500 MHz – 14.5 GHz. (**Nowa struktura EBG z wbudowanym meandrem mostkowym i jej zastosowanie**)*

Keywords: EBG, Embedded Meander Bridge Planar, SSN, SI, PI.
Słowa kluczowe: EBG (electromagnetic bandgap), tłumienie sygnałów, elektrokompatybilność

Introduction

With the trends of high frequency, dense components, and power with fast edge rates and low voltage levels, planar power and ground distribution has become more important for the multilayer printed circuit board (PCB). As the operating frequency is getting higher, the planar structure of the power and ground planes will act like a parallel-plate waveguide which forms a cavity in general package substrate. The resonance modes can be excited by the SSN which is caused by the extensive application of high-speed switching COMS chip in circuits, and by the number of switching ports operating position (on and off) at the same time. Some research showed that the resonance noise propagating between the power and ground planes could cause serious signal integrity (SI) or power integrity (PI) problems for the high-speed circuits [1]–[3]. Moreover, due to the cavity resonance effect between the power/ground planes, the SSN also results in significant radiated emissions or electromagnetic interference (EMI) issues [3].

Many researchers have contributed to the mitigation of SSN. There are two possible ways to reduce the noise. The first way is keeping the PDN impedance very low in a wide frequency range by employing shunt capacitors, except at dc [2]–[3]. Ideally, it's an effective and timely method. However, decoupling capacitors are band-limited which are not effective above the frequency of a few hundred MHz due to the inevitable series inductance in the implementation of the capacitor. The isolation approach that keeps part of the PDN at high impedance is another way to mitigate the PDN noise propagation. The typical isolation approach is the use of the EBG power plane which can provide a wide frequency band gap and can effectively eliminate the SSN on the PCB plane [4]-[6].

Prior to this work, most EBG structures have been developed for large-scale backplane or motherboard applications. Two main research efforts are emphasized for EBG structures applied to SSN suppression [1]. One is stop band bandwidth enhancement because of switching noise from digital circuits covering a wide frequency band. In 2008 the International Technology Roadmap of Semiconductors (ITRS) predicted that the power and on-chip clock are expected to increase to 14.3GHz for the next decade [7]. The other is miniaturization techniques due to the trend of system in package. In this paper an embedded meander bridge planar EBG structure is proposed, which can effectively suppress the SSN from 500 MHz to 14.5 GHz.

Section Ⅱ of this paper describes the topology of the novel EBG structure, followed by the explanation of the design concept; the SSN suppression simulation for the EBG is also discussed in this section. In Section Ⅲ, the effects caused by the EBG power plane on the signal integrity (SI) of the single-ended and differential pair transmission lines are investigated, and some design rules of the signal lines over the EBG power/ground plane pairs are discussed. In Section Ⅳ, the tested novel EBG structure board has been fabricated. The simulated result of broad-band suppression of SSN has been verified with measured result. It is found that the simulated and measured results are similar. The conclusion has been appended in section Ⅴ.

A Structure Design and SSN Suppression

For the planar EBG structure, self- resonance plays the main role in the formation of band gap. The surface impedance of the EBG structure can be made equal to the equivalent parallel LC resonant circuit provided that the size of EBG structure is much less than the wavelength of the signal transmission on it. The center frequency and bandwidth of the band gap is determined by the following,

$$w = 1/\sqrt{LC} \tag{1}$$

$$\Delta w / w = \sqrt{L/C} \tag{2}$$

where L and C are the inductance and capacitance of the planar EBG structure respectively. The value of the L and C can be obtained by the numerical methods. From the equation, it can be seen that the bandwidth is inversely proportional to the value of C. However when the value of C get much smaller, the center stop band frequency will become higher which is not expected. Increasing the value of L can lower the center stop band frequency and widen stop band bandwidth. So supposing that increasing the value of L is much greater than the decreasing value of C, we will get the compact planar EBG structure which has the low center stop band frequency and wide bandwidth of the band gap.

1) The Proposed Embedded Meander Bridge EBG

In our novel EBG structure design, the power plane is etched into embedded meander bridge EBG pattern, while the ground plane is kept continuous. Fig.1 shows the power/ground plane design with 9 (3 by 3) unit cells on the layer FR4 (ε_r = 4.3, $\tan\delta_d$ =0.02) PCB substrate. The

dimension of the substrate is 90 mm × 90mm with 0.4 mm thickness. The unit of embedded meander bridge structure consists of two parts which are a metal patch and four meander bridges as shown in Fig.2. The basic idea behind the design presented here is the use of meander line as connectors between the patches to increase inductance. The capacitance will reduce with increase of space of meander line which shifts the band gap frequency.

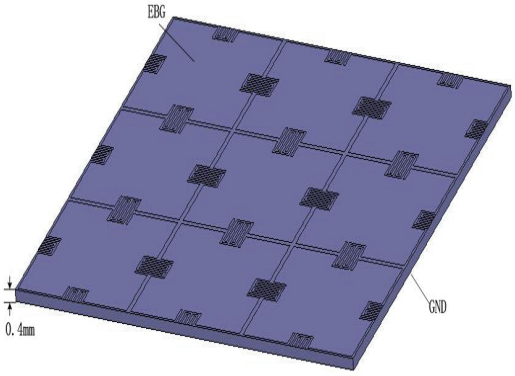

Fig. 1 The embedded meander bridge EBG pattern

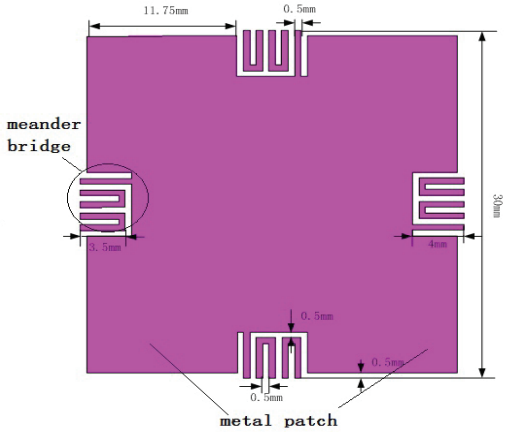

Fig.2 Unit cell of the embedded meander bridge EBG structure

a) Circuit Model of Metal Patch

Let's consider the metal patch part which can be divided into unit cells with a lumped element model for each cell, as described in Fig.3. Each cell consists of an equivalent circuit with R, L, C, and G components for a rectangular structure. The equivalent circuit parameters for a unit cell can be derived from quasi-static models provided the unit cell metal dimension is much lesser than the λ/10, where λ is the guided wavelength of the highest frequency. When the highest frequency is 15GHz, the mesh length of the unit cell metal has been chosen as 2mm.

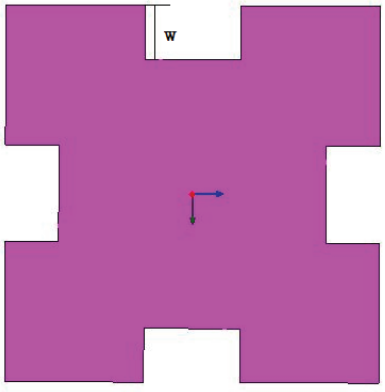

Fig.3 The metal patch of embedded Meander Bridge

The π circuit model of the unit-cell is as shown in Fig.4. The R, L, C and G values in unit cell are calculated by (3).

$$C = \varepsilon_0 \varepsilon_r \frac{w^2}{d}; \quad L = \mu_0 d; \quad R_{dc} = \frac{2}{\sigma_c t};$$

$$(3)\ R_{ac} = 2\sqrt{\frac{\pi f \mu_0}{\sigma_c}}; G_d = wC\tan(\delta)$$

where w, d, σ_c and t are dimension of unit-cell, dielectric thickness, metal conductivity and metal thickness, respectively. Also, ε_0 and μ_0 are permittivity and permeability of free space. R_{dc} denotes the DC resistance of both the power and ground plane for DC current while R_{ac} denotes AC resistance that accounts for the skin effect on both conductors. The shunt conductance G_d indicates the dielectric loss in the material between the planes.

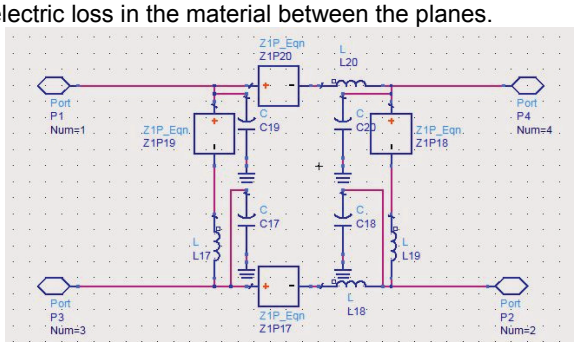

Fig.4 The π circuit model of the metal patch

The corresponding N×N units' circuit model is as shown in Fig.5.

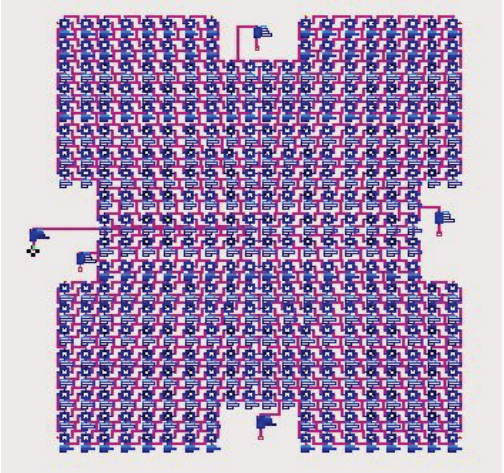

Fig.5 The circuit model of N×N unit of the metal patch

As described above, the bandgap is closely related with the value of C which is mainly determined by the metal patch size. The value will change when we alter the size of the patch. If we vary the width w, the transmission character line of S21 will also vary, for example in Fig.3, when the value of w is 1.5mm, 1.75mm, 2mm, respectively, the transmission character lines of S21 are also varied as shown in Fig.6. From the figure we can see that the bandwidth of the bandgap will become wider when the value of w gets smaller for which the value of C turns lower. We can also change other parameters size of the metal patch, so that the bandgap frequency range will shift to a desirable point. Fig.7 shows both the simulation results using FEM and circuit model for comparison. It can be seen that in the lower frequencies, the results are basically the same while numerical method result using circuit model is a little ahead of the FEM result in the high frequency band.

This is due to the use of approximate parameters which have relative error in the circuit model. However it is not very significant, the results are almost the same as were expected.

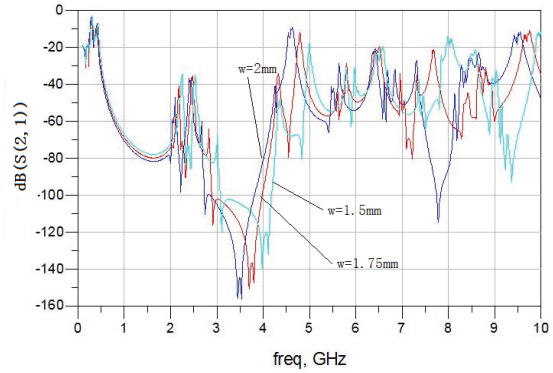

Fig.6 The transmission character lines of S21 when the value of w is 1.5mm, 1.75mm, 2mm, respectively.

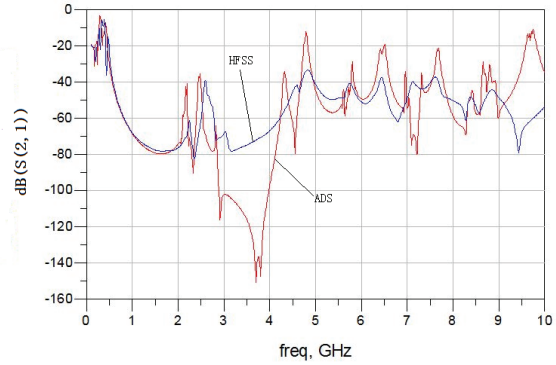

Fig.7 S21 for the simulation results using HFSS and ADS

b) Circuit Model of the Meander Bridge

The meander bridge planar part and its design parameters are shown in Fig.8, and the meander bridge which is placed on top of a 0.4mm dielectric substrate consists of metallic arms and metallic bridges connecting arms as shown in Fig.9. Its circuit model is shown in Fig.10.

It is assumed that all traces in the meander have the same parameters of width (M_W), separation gap between adjacent arms (M_G) and arm length (M_L). In Fig.10, the inductor is the dominant element in this model up to the first self resonant frequency. The capacitors model is results of the parasitic effects. It should be noted that in this model, the effect of right angled bends in the meander line has not been considered. The effect of these bends becomes more pronounced at much higher frequencies than the range of interest considered in this work.

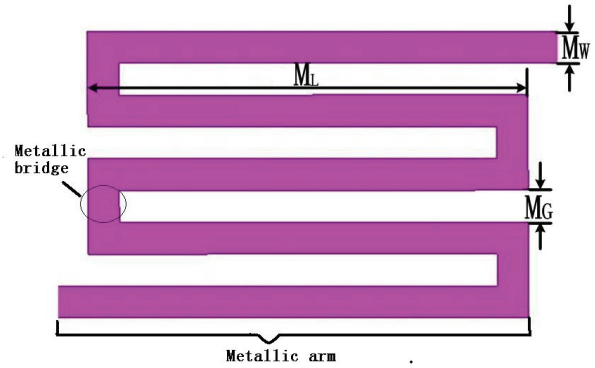

Fig.8 The meander bridge planar part

Using Greenhouse formulas [8] and image theory [9], the total meander line inductance can be calculated by the following equation,

$$L = L_P + L_{MIP} \tag{4}$$

where L_p is the self-inductance of meander pattern trace and L_{MIP} is the mutual inductance between the meander line and its ground image (See Fig.11 and Fig.12).

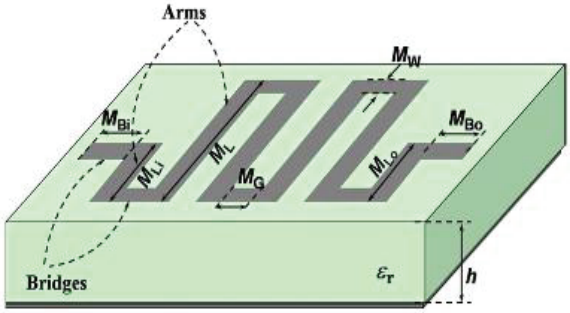

Fig.9 3-D distribution of the meander bridge.

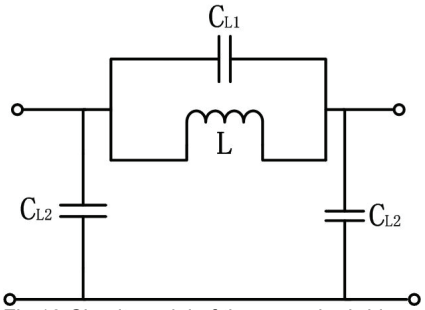

Fig.10 Circuit model of the meander bridge

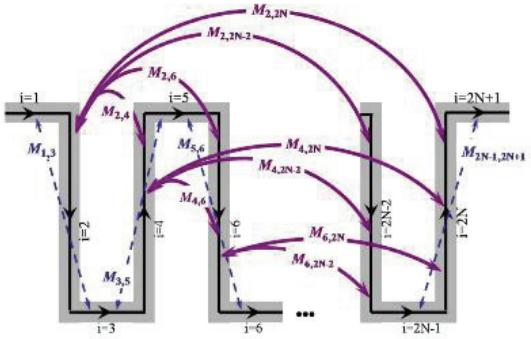

Fig.11 Magnetic coupling between meander lines.

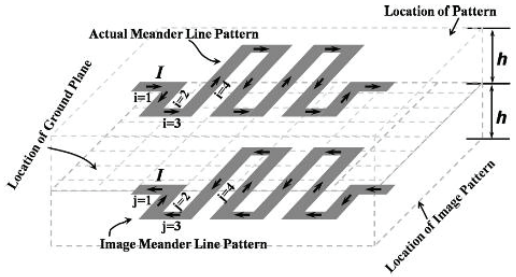

Fig.12 The meander line and its ground image

There are two types of parasitic capacitances in the meander line model, as shown in Fig.13. C_{L1} represents the equivalent capacitance resulting from series of gap capacitances C_{g_j} produced by the N-1 consecutive inter-arm gaps and it can be computed as

$$C_{L1} = 1/\sum_{j=1}^{N-1}(1/C_{g\_j}) \tag{5}$$

where C_{g_j} is the parasitic interline capacitance between two coupled adjacent arms.

C_{L2} is the equivalent capacitance resulting from the sum of parasitic capacitance between the middle strip and the ground. All the detailed calculations of L, C_{L1}, C_{L2} can refer to [10].

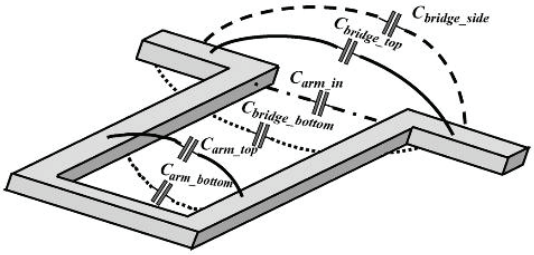

Fig.13 Parasitic capacitances in the meander line

As mentioned above, the band gap can be moved to other values by changing the effective L. As for the meander bridge, inductance plays the main role in its circuit model and its equivalent value is determined by the size of the meander bridge. Therefore, we can shift the band gap range of novel EBG structure by changing the parameters size of the meander bridge. For example here we take the meander bridge length as M_L and the meander bridge width as M_W respectively.

First, we vary the value of the M_L from 2000um to 12000um, the changing trend of the total inductance value of the meander bridge can be found as in Fig.14(1). It can be seen that the inductance is approximately proportional to the increase of value of M_L. The longer the meander bridge is, the greater the inductance. Similarly, it also found from Fig.14(2) that the value of inductance changes in accordance with the value of M_W. However, the inductance becomes smaller when the value of M_W changed to larger.

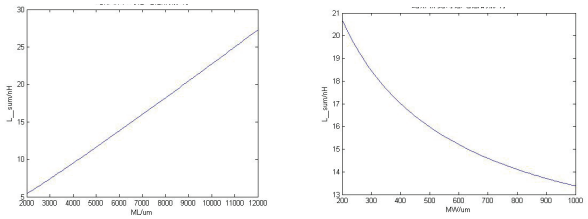

Fig.14 (1)The changing trend of the total inductance value with the length (M_L) of the meander bridge. (2) The changing trend of the total inductance value with the width (M_W) of the meander bridge.

According to the discussions above, the shape and size of the EBG planar can be changed, and the expected optimal structure can be found. At present the target for EBG design is to lower the center stop band frequency and wider band width of band gap.

2) Study of SSN Suppression

The EBG structure can be applied in eliminating the SSN in the power and ground planes. Fig.2 shows the designed novel EBG structure and the dimensions are marked in the unit cell in detail. Using the model in Fig.15 and adding three ports at the location we can do simulation. Taking the planar center point (0,0) as the reference point, excitation point is in the position of reference point Port1 (0mm, 0mm), receiver is in the position of Port2 (30mm, 30mm) and Port3 (0mm, 30mm) respectively. The simulation result for the transmission characteristics between Port 1 and Port 2 are shown in Fig.17. The results indicate that the valid -30 dB suppression bandwidth is broadened from 500MHz to 14.5 GHz. As at present the general SSN is ranges from 600MHz to 4.6GHz, so the proposed novel EBG structure can eliminate the SSN effectively at the lower range of 4GHZ while it can also suppress the noise at the higher frequencies than 4.6 GHz which is expected.

Here two different cases have been compared which are shown in Fig.18. In the first case (Fig.17), the signal propagates on the power and ground planes with respect to the power plane of an EBG patterned plane. In the second case, the signal is referenced to two solid planes. The ports in the two cases are on the same corresponding locations. Comparing the result of EBG board with the solid board, it is clearly seen that the proposed EBG power/ground planes significantly eliminate the SSN with, on average, over -30dB suppression in a broad-band frequency range.

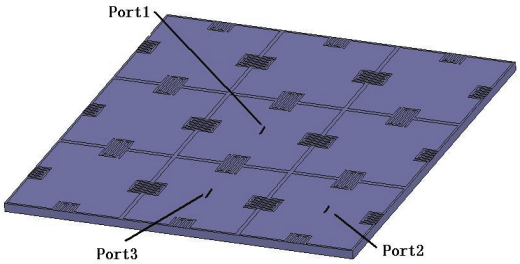

Fig.15 Model with EBG patterned plane.

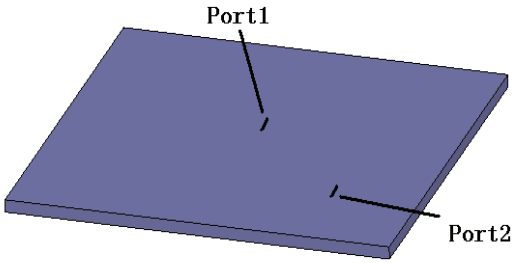

Fig.16 Model with solid plane.

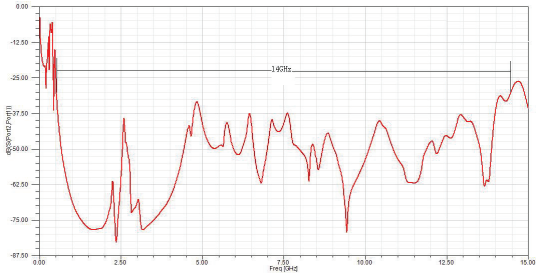

Fig.17 S21 of the embedded meander bridge planar EBG.

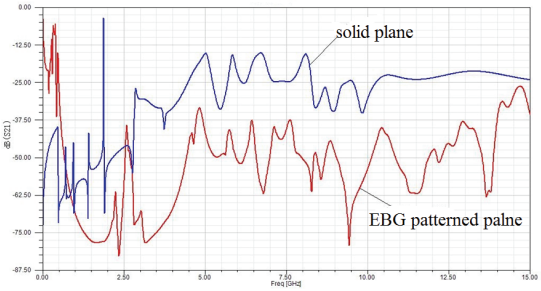

Fig.18 Simulation comparison between EBG patterned plane and solid plane.

As shown in Fig.15, the transmission characteristics have been simulated between Port1 as the excitation end and both Port2 and Port3 as the receiving end. The result is shown in Fig.19. It is seen that the proposed design EBG provides the similar broad-band SSN suppression for different positions of the noise. This behaviour demonstrates that the proposed power/ground planes can Omni-directionally eliminate the GBN on the power plane.

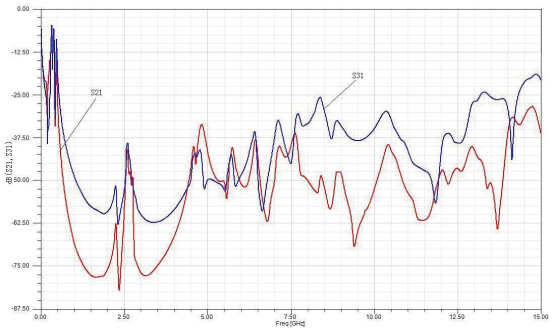

Fig.19 Transmission characteristics with same excitation and different receiving ends.

B Signal Integrity Effects

Although the proposed EBG power and ground planes design show excellent performance on eliminating the SSN at the ranges of broad-band frequency, however the power plane with etched slots would degrade the signal quality for the signal traces referring to the imperfect power plane [11]. In this section, the impact of the proposed EBG power plane on the SI and two possible solutions to improve the SI are discussed.

1) Effects of Bandgap Behavior on Single-End Traces

How the band gap affects the electrical transmission characteristic of the single-end signal traces between the power plane with an EBG structure and the ground plane has been investigated in this paper. Fig. 20(a) and (b) show the model of single-ended trace and its side face, and the length of trace is 70 mm passing from the first (top) layer to the fourth (bottom) layer, with one via transition along the signal path. The second and third layers are the power plane which is used EBG etched and solid ground plane, respectively. The depth between the first layer and the power plane is 0.1mm, and for the power plane and the ground plane, ground plane and bottom layer is 0.4mm, 0.1mm, respectively. The width of the line is 1mm.

It is known that via transitions and imperfect reference plane are two of the main factors to influence the signal quality for the high speed signals. This setup in Fig.20 tried to evaluate the impact of the novel EBG power plane on the signal quality for the signals, both referring to the power plane and via transitions. The traces are designed as 50 Ohm for the single-ended signal impedance. Eye pattern for evaluating the signal quality of the single-ended is shown in Fig.21 (a). For comparison, the case of the single trace on the solid power and ground planes has been done. The result is shown in Fig.21 (b). From the result it is seen that the eye diagram significantly shrinks for the structure with EBG power plane. This is mainly due to the strong reflection arising from this non-uniform EBG patterned power plane.

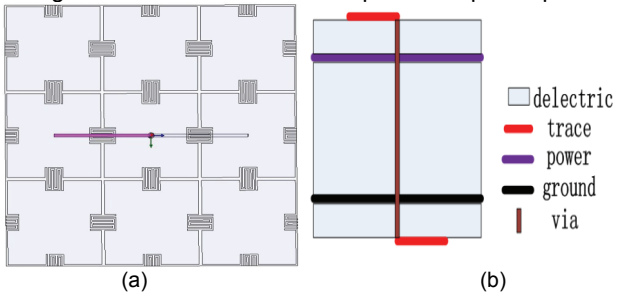

(a) (b)

Fig.20 (a) Model of single-ended trace; (b) Side face

2) Differential Pair

In order to improve the signal quality, a differential signaling approach is adopted. In this example the traces are designed with a differential impedance of 100 Ohm as shown in Fig. 22(a). The width of the lines is 2mm, and the spacing between the two lines is 3mm. The other parameters for the model of Fig.22 (a) are same as the model of Fig.20. Fig22 (b) shows the different side face of the model that has been discussed here. The eye diagram for the differential pair lines model is shown in Fig 23. It can be seen that the signal quality has greatly improved if compared with that of the single ended feeding as shown in Fig.21 (a).

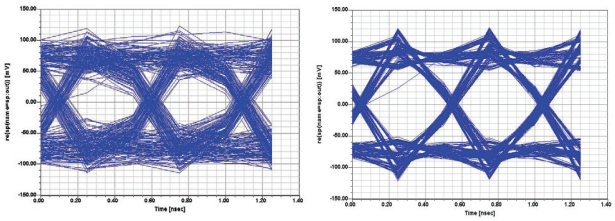

(a) (b)

Fig.21 (a) Eye pattern with EBG patterned plane; (b) Eye pattern with solid plane.

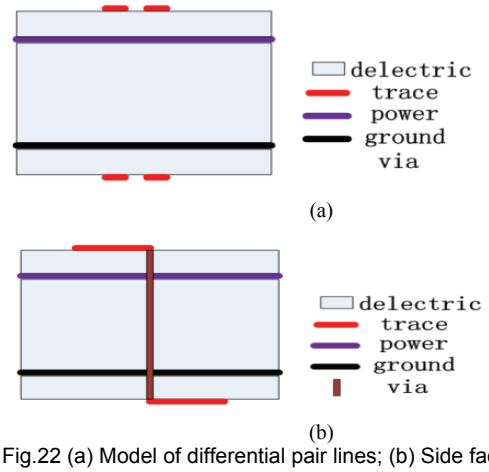

Fig.22 (a) Model of differential pair lines; (b) Side face

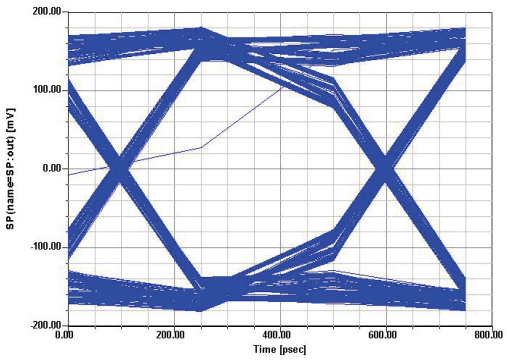

Fig.23 Eye pattern of differential pair lines

It is believed that this mild degradation of the eye diagram as shown in Fig.21 (a) is acceptable in practical high-speed circuits. Furthermore, we can improve the SI through suitable components placement and layout designs, such as routing lower speed signals on the top layer and keeping high-speed traces on the bottom layer, or avoiding the high-speed signals crossing the EBG cells, the overall SI performance will be significantly better than the previously simulated case. However, if long and high-speed signals are still necessary on the first layer, the differential signaling approach is a good solution.

C Experiment Validations

In order to validate the result of S_{21}, an EBG test board has been manufactured, as shown in Fig.24. A voltage network analyzer (VNA) has been used to do the measurement of the designed structure. The measurement result of the manufactured EBG test board is shown in Fig.25. We can conclude that the SSN suppression performance of the proposed EBG structure confirms well by conducting simulations and measurements in the frequency domain. Here the dash line refers the simulation result and the solid line is the measurement result, and the simulated and measured stopband bandwidth for 9 unit cell board is 14GHz. It can also be seen that there are slightly discrepancies between the measured bandwidth and the simulated bandwidth and the measured center frequency and the simulated center frequency of the stopband. The reason could be that the conductor loss and the dielectric dispersion broaden the stopband at a higher frequency range.

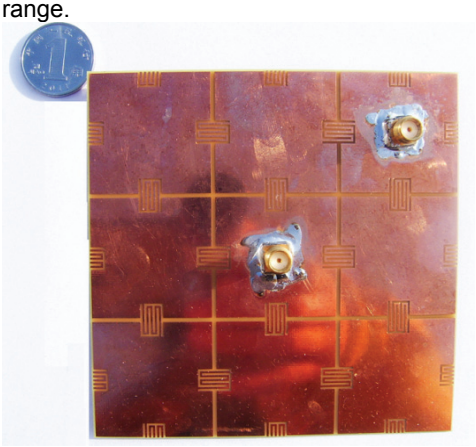

Fig.24 EBG test board

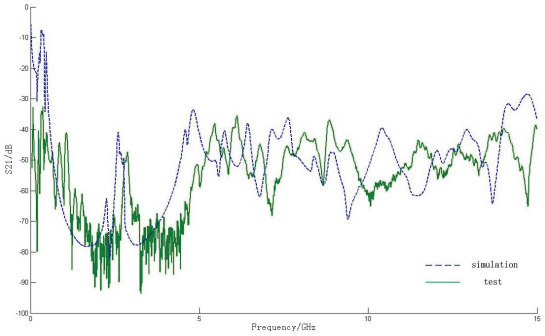

Fig.25 Comparison between the measurement result and simulation result.

D Conclusions

This paper describes the design rule of the novel EBG. The simulation and the experimental verification proves that the novel embedded meander bridge planar EBG structure is a promising method for suppressing ultra-wideband (UWB) simultaneous switching noise (SSN) in power/ground plane pairs and overcomes the limitations of typical EBG structures, such as limited bandwidth and lower start cut-off frequency. Although coplanar EBG structures can degrade the Signal Integrity (SI) quality, they can still be applied as reference planes if we carefully follow the design rule of traces on power plane and pay more attention to the signal integrity on the traces analysis.

Acknowledgments

This work was supported in part by NSFC under Grant No. 60831001.

REFERENCES

[1] Tzong-Lin Wu and Hao-Hsiang Chuang, "Overview of Power Integrity Solutions on Package and PCB: Decoupling and EBG Isolation," IEEE Trans. Electromagn. Compat., vol. 52, no.2, pp. 346–356, May 2010.

[2] J. Fan, J. L. Drewniak, J. L. Knighten, N. W. Smith, A. Orlandi, and T. P. Van Doren "Quantifying SMT decoupling capacitor placement in DC power-bus design for multilayer PCBs," IEEE Trans. Electromagn. Compat., vol. 43, no.4, pp. 588–599, Nov. 2001.

[3] J. Fan, W. Cui, J. L. Drewniak, T. P. Van Doren, and J. L. Knighten, "Estimating the noise mitigation effect of local decoupling in printed circuit boards," IEEE Trans. Adv. Packag., vol. 25, no.2, pp. 154–165, May 2002.

[4] T. Kamgaing and O. M. Ramahi, "A novel power planes with integrated simultaneous switching noise mitigation capability using high impedance surface," IEEE Microw. Wireless Compon. Lett. vol. 13, no.1, pp. 21–23, Jan. 2003.

[5] T. L. Wu, Y. H. Lin, T. K. Wang, C. C. Wang, and S. T. Chen, "Electromagnetic bandgap power/ground planes for wideband suppression of ground bounce noise and radiated emission in high-speed circuits," IEEE Trans. Microw. Theory Tech., vol. 53, no. 9, pp. 2935-2942, Sep. 2005.

[6] L. Li, Q. Chen, Q. Yuan, and K. Sawaya, "Ultra-wideband suppression of ground bounce noise in multilayer PCB using locally embedded planar electromagnetic bandgap structures." IEEE Antenna Wireless Propag. Lett. vol. 8, pp. 740–743, 2009.

[7] International Technology Roadmap for Semiconductors. London, U.K. (2008). [Online]. Available: http: //www. itrs.net/.

[8] S.Shahparnia and O.M.Ramahi,"Electromagnetic interference (EMI) reduction from printed circuit boards(PCB) using Electromagnetic bandgap structures," IEEE Trans. Electrom., Compat., Vol.46, no.4, pp.580-586, Nov, 2006.

[9] T.Kamgaing and O.M.Ramahi,"Design and modeling of high-impedance electromagnetic surface for switching noise suppression in power planes," IEEE Trans.Electrom., compat., vol.47 no.3, pp.479-489. Aug, 2005.

[10] K.C.Gupta, R. Garge, I. Bahl, and P. Bhartis, Microstrip Lines and Slotlines. Norwood, MA: Artech House, 1996.

[11] Ramahi, O.M., Mohajer-Iravani, B., Qin, J.; Shahparnia, S., and Kamgaing, T., "EMI Suppression and Switching Noise Mitigation in Packages and Boards using Electromagnetic Band Gap Structures," Signals, Systems and Electronics, 2007. ISSSE '07. International Symposium on, vol., no., pp.271-274, July 30 2007-Aug, 2007.

Authors: *Zhaowen Yan received the Ph.D degree in electrical engineering from Xi'an Jiaotong University, China, in 1999. For many years, his research activity was focused on the electromagnetic field computation and EMC analysis. He has published over 50 conferences and journal papers and 7 monograph on electromagnetic theory. He was awarded a gold prize of Ministry of Education of PRC in 2003 and Ministry of Industry and Information Technology of PRC in 2011.*

Zhaowen YAN is an Associate Professor with the School of Electronic and Information Engineering of Beihang University, Beijing, China (phone: +86-10-82339410; fax: +86-10-82317224; e-mail: yanzhaowen@buaa.edu.cn).